Role of the nanoscale in catalytic CO oxidation by supported Au and Pt nanostructures

Sergey N. Rashkeev,[1,2,*] Andrew R. Lupini,[1,†] Steven H. Overbury,[3]
Stephen J. Pennycook,[1,2] and Sokrates T. Pantelides[2,1]
[1]*Materials Science and Technology Division, Oak Ridge National Laboratory, Oak Ridge, Tennessee 37831, USA*
[2]*Department of Physics and Astronomy, Vanderbilt University, Nashville, Tennessee 37235, USA*
[3]*Chemical Sciences Division, Oak Ridge National Laboratory, Oak Ridge, Tennessee 37831, USA*
(Received 21 March 2007; revised manuscript received 11 June 2007; published 27 July 2007)

Experiments have found that the catalytic activity of Au increases sharply for supported nanoparticles smaller than 5 nm, while Pt exhibits the opposite behavior. Several authors, seeking to explain the nanoscale Au activity, reached conflicting conclusions, attributing it to different nanoscale features or to a particular bilayer structure that is independent of size. Here, we report an extensive theoretical study of a large ensemble of TiO_2-supported Au and Pt nanoparticles and show that several nanoscale features *collectively* result in the observed contrasting behavior. Low coordination is accompanied by bond weakening in Au and strengthening in Pt, while perimeter sites are active only for Au. Though there are orbital-occupancy differences for catalytically active and inactive configurations, there is insignificant variation in physical-charge transfer. Finally, we report atomically resolved *Z*-contrast images that confirm bond weakening in catalytically active TiO_2-supported Au nanoparticles.

DOI: 10.1103/PhysRevB.76.035438 PACS number(s): 82.65.+r

I. INTRODUCTION

Platinum[1–4] and most other noble metals[5] are good catalysts for CO oxidation. Gold was widely believed to be an exception until the striking discovery by Haruta *et al.* that supported Au nanoparticles *smaller than* 5 nm are more active than other noble-metal catalysts for low-temperature CO oxidation.[6] In contrast, supported Pt nanoparticles smaller than 5 nm either show decreased catalytic activity[1,2,4] or no strong size dependence[3] for CO oxidation. Subsequent investigations that focused on Au reached conflicting conclusions, attributing the enhanced activity to *different* nanoparticle features (perimeter sites,[1,7] low-coordination atoms,[8–12] charge transfer,[7,13–19] dynamic structural fluxionality,[18,19] nonmetallic properties,[20,21] and oxidation state[22]). A size-independent mechanism based on bilayer structures has also been proposed.[23,24] However, the contrasting behavior of Pt was not addressed in the same extent. Thus, the issue of how the same nanoscale feature, e.g., low-coordination atoms, results in opposite trends in the two systems remains open.

Here, we report a theoretical study of a large ensemble of TiO_2-supported Au and Pt nanoparticles and show that several nanoscale features collectively result in the observed contrasting behavior. We find that low coordination is necessary for the Au activity, but another feature, which is present in Au but not Pt, is also essential. Bonding of either a CO or an O_2 molecule to a Au nanoparticle is accompanied by weakening of the Au–Au bonds, which facilitates the catalytic reaction. In contrast, Pt–Pt bonds in Pt nanoparticles become more rigid and the catalytic reaction is inhibited. For similar reasons, Au-nanoparticle perimeter sites are very active, while Pt-nanoparticle sites are not. We also found that orbital-occupancy variations are relevant to catalytic activity, but transfer of physical charge is minimal and does not play a significant role. In addition, our calculations confirm that the bilayer Au structures of Refs. 23 and 24 are catalytically active. The origin of this catalytic activity appears to be either "itinerant reconstruction" or local surface-oxygen fluctuations that cause the appearance of both low-coordination Au sites *and* bond weakening, precisely as in nanoparticles. Similar Pt structures are not catalytically active. Finally, we report atomically resolved *Z*-contrast images that corroborate the presence of bond weakening in catalytically active TiO_2-supported Au nanoparticles.

II. THEORY AND SIMULATIONS

In order to investigate the role of different nanoparticle features in the CO-oxidation catalytic activity, we constructed an extensive ensemble of Au and Pt nanoparticles on TiO_2 substrates and optimized their geometries using density-functional theory. Calculations were performed on a four-layer-thick TiO_2(110) rutile slab and a three-layer-thick (101) anatase slab. Both slabs were terminated by nonpolar surfaces. Large, periodically repeated supercells were used ($13.0\times12.4\times23.5$ Å^3 for rutile and $18.9\times12.7\times23.5$ Å^3 for anatase). The vacuum layer between slabs was >12 Å.

Gold nanoparticles containing between 5 and 35 atoms on a titania slab were constructed as follows. In agreement with prior calculations,[25] we first verified that true chemisorption of gold nanoparticles requires at least one oxygen surface vacancy. We then started with five gold atoms placed above an oxygen vacancy and relaxed all atoms in the nanoparticle and top surface layers until the quantum-mechanical force on each atom became smaller than 0.02 eV/Å. Larger gold nanoparticles were constructed by repeatedly adding a single gold atom and allowing the structure to relax again. The supercells are sufficiently large so that even 35-atom nanoparticles interact with their neighbors only weakly. Though several different initial configurations were adopted, in each case seeking a low-energy structure, a systematic search for the lowest-energy structure was not pursued for several reasons. First, the experimental formation of nanoparticles is not necessarily an equilibrium process, so that metastable

configurations are likely to form; second, one can never ensure that the truly lowest-energy structure is found; and third, our objective was to explore the role of coordination, charge transfer, etc., so that it was more useful to construct an ensemble of nanoparticles with diverse local bonding and coordination numbers. Once we had an ensemble of stable gold nanoparticles, all gold atoms were replaced by Pt and the structures were relaxed again.

For simulation of processes on larger nanoparticles, quasi-one-dimensional periodic rodlike structures containing a well-defined boundary between the nanoparticle and the substrate were used. Our objective was to have stable structures with a well-defined "perimeter" between the nanoparticle and the surface where we could explore catalytic activity.

The calculations were based on the generalized gradient approximation (GGA) for exchange and correlation, and plane waves.[26] We used the GGA of Perdew *et al.*,[27] which gives good results for chemisorption of molecules at transition-metal surfaces. Ultrasoft scalar relativistic pseudopotentials and the VASP code[28] were used. The energy cutoff for the plane-wave basis was set at 400 eV, and all integrations over the Brillouin zone were done using the Monkhorst-Pack scheme with one **k** point in the relevant irreducible wedge.[29] Inclusion of additional **k** points was found to have minimal effect on the total-energy differences of interest here.

The calculations did not include spin polarization because there was no intent to explore magnetic properties. Test spin-polarized calculations were performed, especially with O and O_2 adsorbed on the nanoclusters, to ensure that total-energy differences of interest here were not significantly affected. Once the structures are relaxed, total-energy differences between distinct magnetic orderings are much smaller than the reaction energies and activation barriers that we obtain for catalytic activity.

Adsorption energies for CO and O_2 at various sites on the nanoparticles, including perimeter sites, were calculated by optimizing local geometries. Energy barriers for CO oxidation were calculated using the nudged-elastic-band method.[30] This method searches a wide range of pathways to produce barrier values that progressively approach the true barrier. The results (see below) exhibit a systematic behavior with coordination number and, in the case of Pt, the calculated results agree well with the value for Pt(111) from previous work.[31,32] The barriers for Au nanoclusters roughly tend toward zero for small coordination numbers, suggesting that the calculated barriers, though in principle upper bounds, are, in fact, close to the true values. Further validation of the computed barriers is that the experimentally measured apparent activation energies range from about 0.2 to 0.3 eV,[33] comparable to barriers we calculated for Au coordination numbers of 3–5. For statistical analysis of the CO and O_2 binding energies and the reaction barriers (Fig. 1), we used at least eight different configurations for each coordination number n of the Au atoms to which the oxygen molecule was attached. No significant differences were found for nanoparticles adsorbed on rutile or anatase TiO_2 substrates.

On virtually all Au particles, O_2 adsorbs as a molecule. Adjacent O_2 and CO molecules react to produce CO_2, which desorbs, leaving a bonded O atom. On Pt surfaces[31,32] and nanoparticles, O_2 adsorbs strongly with a stretched O–O bond that dissociates easily, allowing adjacent O atoms and CO molecules to react.

III. RESULTS AND DISCUSSION

A. Site coordination number and $CO+O_2$ reaction barrier

In Fig. 1, we summarize our results for reaction barriers (E_r) and O_2 desorption energies (E_d). CO desorption energies are always larger and are not shown. This figure reveals a crucial difference between Au and Pt nanoparticles. Upon adsorption, the neighboring Au–Au bonds become longer and weaker [Fig. 1(a)], *making the rotation and stretching needed for the reaction less energetically costly* [Fig. 1(b)]. Such weakening (akin to "structural fluxionality"[18,19]) does not occur at the corresponding Pt–Pt bonds [Fig. 1(d)]; i.e., the Pt nanoparticles are more rigid, resulting in higher reaction barriers because it is harder for the strongly adsorbed molecules to move and interact [Fig. 1(e)]. Thus the reaction barrier decreases at low-coordination Au sites [Fig. 1(c)] and increases at low-coordination Pt sites [Fig. 1(f)].

The most striking result for Au nanoparticles is the crossing of the E_r and E_d curves as a function of the average Au-Au coordination number n of the two Au atoms to which O_2 is bonded [Fig. 1(c)]. Reaction is favored over desorption only at sites with average coordination $n<5$, when $E_r<E_d$, i.e., the time for the reaction to occur is shorter than the residence time of the adsorbed O_2 molecule. At perimeter sites, O_2 molecules bind more strongly and catalytic activity is favored even with $n=6$ or 7 because the bridge bond[17] to the TiO_2 substrate helps weaken the O–O bond [Fig. 2(a)]. As shown in Fig. 1(c), reaction barriers on the perimeter are lower and also decrease with decreasing coordination. These results are in good agreement with recent experimental work,[34] in which a combination of extended x-ray-absorption fine structure and scanning transmission electron microscopy was used to analyze the catalytic activity of Au atoms with different coordinations.

The behavior of Pt nanoparticles is distinctly different. Figure 1(f) shows that we always have $E_r<E_d$, so that catalysis is always possible in principle (for large nanoparticles, our E_r values approach the known value at Pt surfaces[31,32] ~0.8 eV). However, the absolute values of E_r and E_d both become larger with decreasing coordination (unlike Au, where E_r decreased). In addition, perimeter sites for Pt particles are not catalytically active as O_2 molecules dissociate and the O atoms bind too strongly. The larger binding energies of CO and O_2 to Pt nanoparticles [Fig. 2(b)] relative to flat surfaces implies longer residence times, meaning that active sites on Pt nanoparticles could be blocked or even poisoned relatively easily.

B. Coordination number and charge transfer

We further searched for a possible correlation between charge transfer to the O_2 molecule and the catalytic activity. It is customary to assign a value of physical charge to individual atoms by integrating the charge in a particular volume, typically a sphere, as in the Mulliken scheme,[35] but the

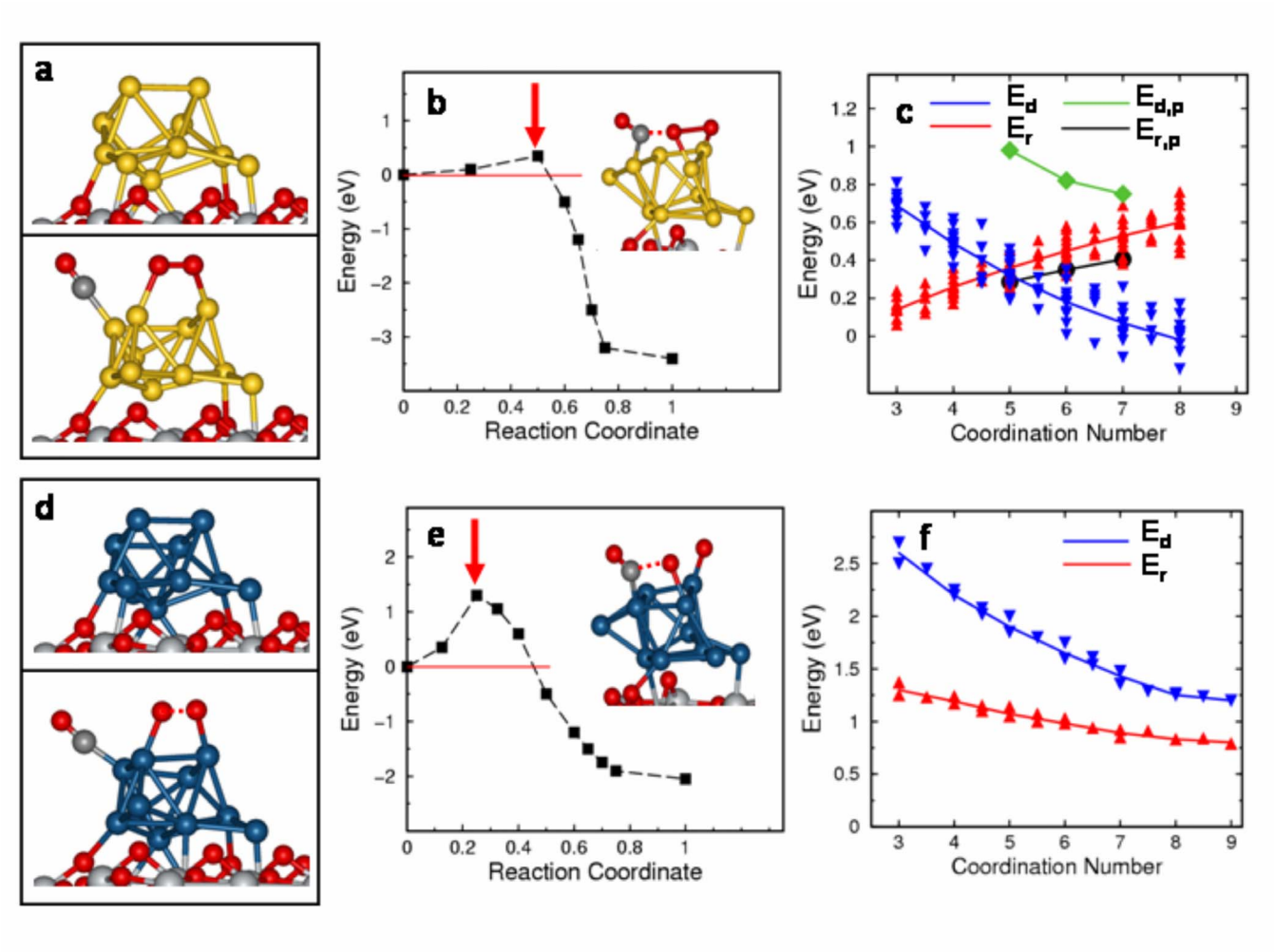

FIG. 1. (Color online) Adsorption and reaction of O_2 and CO molecules on TiO_2-supported [(a)–(c)] Au and [(d)–(f)] Pt nanoparticles. Ti is shown in light gray, O in red, Au in yellow, Pt in blue, and C in dark gray. (a) The relaxed configuration of 11-atom supported Au nanoparticle before (upper panel) and after (lower panel) adsorption. Three Au–Au bonds are now so stretched that they are no longer shown in the schematic, facilitating the rotations and bending needed for the reaction. The O-O distance increases to 1.39 Å here. (b) The reaction energy profiles and schematics of the nanoparticle at the transition state (arrowed). (c) The desorption energy E_d of an O_2 molecule and the reaction barrier E_r as a function of the average coordination number n of the two Au atoms to which the O_2 molecule is attached. Points correspond to different adsorption sites and/or different nanoparticles located over oxygen vacancies in rutile (110) or anatase (101) surfaces. The average curves of E_d and E_r (bold solid lines) are shown. The lines $E_{d,p}$ and $E_{r,p}$ correspond to the desorption energy and the reaction barrier for the bridge-bond perimeter sites of Au clusters. [(d)–(f)] The corresponding figures for Pt nanoparticles. The O-O distance is 1.48 Å. However, no Pt–Pt bonds are eliminated by the adsorbed molecules resulting in a *higher* reaction barrier.

choice of radius is not unique. Nonspherical volumes have also been introduced (e.g., Ref. 36), but they also lead to ambiguities and difficulties (see, e.g., Ref. 37). Another common practice is to examine the occupation of basis orbitals centered on individual atoms without concern about the physical location of the corresponding electron density. However, atom-centered basis orbitals typically have nonnegligible amplitudes over atoms at neighboring sites.

In order to avoid such ambiguities and difficulties, we clearly distinguished between physical charge and orbital occupation and examined the issue of charge transfer by integrating the total charge within spheres of different radii centered on adsorbed O atoms. We found that, though there is a difference in *orbital occupancies* for catalytically active and inactive configurations, there is minimal variation in the

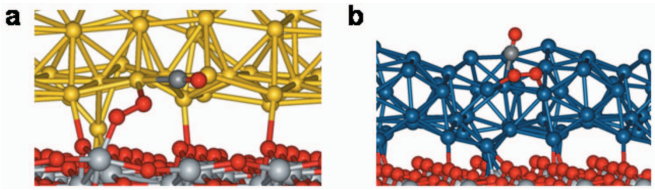

FIG. 2. (Color online) Quasi-one-dimensional Au or Pt structures on TiO_2. (a) O_2 molecules preferentially form bridge bonds between perimeter Au sites and the substrate. The O–O bond in this configuration is stretched to 1.45 Å, which lowers the oxidation reaction barrier. (b) For a similar Pt structure, the O_2 molecule survives without splitting on the top of the particle only (and splits at the perimeter sites).

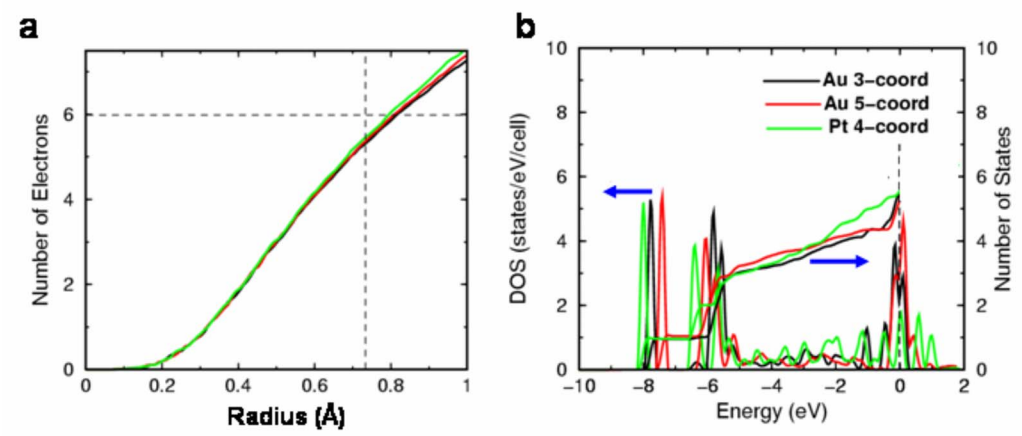

FIG. 3. (Color online) (a) The integrated radial charge around one of the O atoms in O_2 molecules attached to Au (black, threefold coordinated; red, fivefold coordinated) and Pt atoms (green, fourfold coordinated). The horizontal line corresponds to the number of valence electrons per O atom and the vertical line to the atomic radius of an O atom (taken as 0.73 Å). (b) The O_2-projected partial density of states (DOS) in a sphere of radius 0.73 Å and the integrated DOS (number of states) per O atom.

physical charge. In Fig. 3, we show the results for three representative examples: O_2 attached to threefold coordinated Au atoms, to fivefold coordinated Au atoms, and to fourfold coordinated Pt atoms.

More specifically, in Fig. 3(a), we show the total integrated charge around an O atom in each of the three O_2 molecules as a function of the integration radius. It is clear that the total charge in all three cases is essentially the same. The same result holds for all other cases we examined (within about 0.2 electrons).

In Fig. 3(b), we examine the projected density of states in a radius of 0.73 Å (the covalent radius of O) for each of the three O atoms considered above. One interesting feature is that the antibonding $2\pi^*$ O_2 orbital is very close to the Fermi level and becomes increasingly occupied with decreasing Au coordination number. For Pt, this orbital splits due to the strong interaction with the Pt nanoparticle. Nevertheless, these density of states (DOS) differences do not translate into differences in charge transfer. We demonstrate this result by integrating the projected DOS from the bottom of the valence band up to an energy E. The resulting curves, as functions of E, cross the Fermi level with essentially the same value [Fig. 3(b)], demonstrating once more that the total charge in the atomic sphere is the same in all cases. Figure 3(a) demonstrates that this result is independent of the choice of radius, up to radii that begin to sample the neighboring sites.

The above results suggest that correlations of catalytic activity with formal oxidation state observed experimentally[22] represent differences in the local bonding (that result in different projected DOS) but not differences in charge transfer. There is some variation in the integrated charge, but the value stayed within ±0.2 electrons of that for an O atom in a free O_2 molecule. The key point is that, though orbital occupancies are different for different local geometries, the physical charge stays roughly the same. When considering the ensemble of nanoparticles, we did not find a significant correlation of physical-charge transfer with catalytic activity for either Au or Pt.

C. Comparison with experiment

The theoretical results we presented above identify the atomic-scale mechanisms that underlie the catalytic activity for both Au and Pt. Though more complex processes involving CO and O_2 molecules cannot be ruled out, we sought further corroboration of our theoretical results by making a more direct comparison between theory and available experimental data as follows. We determined the statistical distribution of low-coordination sites (n=3,4,5) as a function of nanoparticle size using the relaxed structures of our ensemble of supported nanoparticles. The result for Au particles is shown in Fig. 4. The most striking result is that particles smaller than 1–2 nm are needed to get a significant number of low-coordination sites. However, Au nanoparticles on TiO_2 are also catalytically active at perimeter sites [Fig. 1(c)]. As the nanoparticle size decreases, the perimeter-to-surface-area ratio increases, so that we expect a rise in the contribution from perimeter sites as well.

In order to compare the relative contributions of low-coordination and perimeter sites, we adopt a simple model

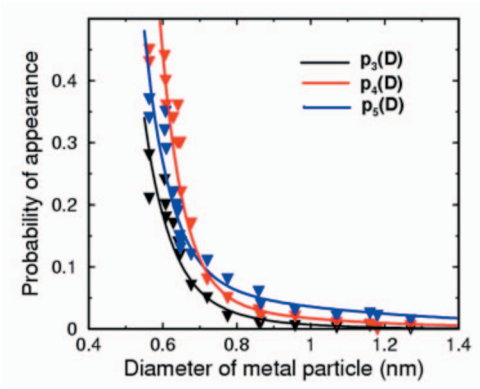

FIG. 4. (Color online) The probability of having a three-, four-, or five-coordinated Au atom on a nanoparticle of a particular diameter, obtained from our ensemble of supported nanoparticles. The solid curves are fitted exponentials.

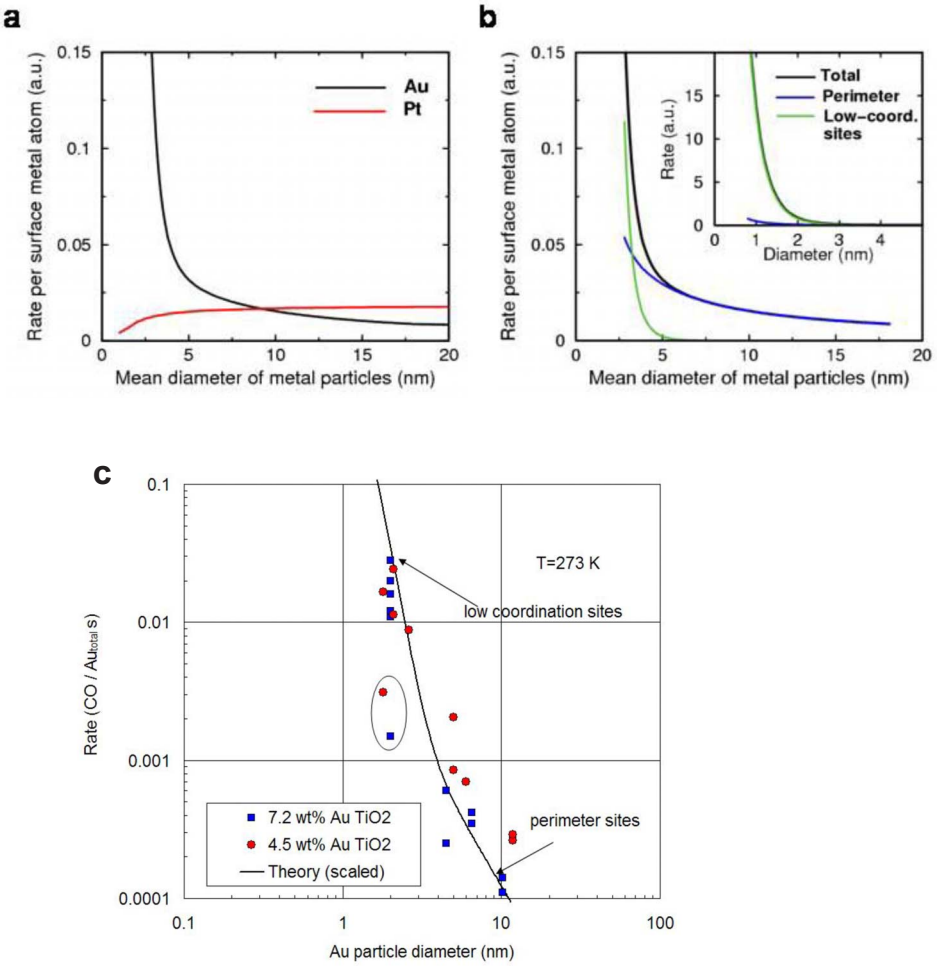

FIG. 5. (Color online) (a) Theoretical simulation of catalytic activity (in arbitrary units) for Au/TiO_2 at 273 K (black) and for Pt/TiO_2 at 437 K (red). (b) The two contributions (and their sum) to the total reaction rate for Au/TiO_2 at 273 K. The rates for the perimeter mechanism (blue) and for the low-coordination sites (green) show a crossover at 3 nm. Below 2 nm, the rate is dominated by low-coordination sites (inset). (c) Comparison of experimental size dependence (points) from Ref. 33 with the predicted dependence (curve). The theoretical rate curve is scaled arbitrarily.

based on the assumption that the rate limiting step is the reaction between coadsorbed CO and O_2 molecules. We distinguish between perimeter sites, where catalysis occurs with reaction barrier $E_{r,p}$, and the remaining sites, where catalysis occurs with reaction barrier $E_{r,n}$, where n is the local coordination. Assuming hemispherical particles, the ratio of perimeter atoms to surface atoms is $2a/D$, where a is the Au-Au interatomic spacing and D is the nanoparticle diameter. We then express the catalytic rate per surface atom as

$$R(D) \propto \frac{2a}{D} e^{-E_{r,p}/kT} + \left(1 - \frac{2a}{D}\right) \sum_n p_n(D) e^{-E_{r,n}/kT}, \quad (1)$$

where $p_n(D)$ is the probability that a particle of diameter D has a site with average coordination n. The first and second terms correspond to catalysis at perimeter sites and low-coordination nanoparticle sites, respectively. We used average values of $E_{r,n}$ from Fig. 1(c) and the p_n curves from Fig. 4, and illustrate the two curves, multiplied by arbitrary scaling factors, in Fig 5(a). This simple model reproduces the significant *trends* of the size-dependent behavior for both Au and Pt nanoparticles described in Ref. 1 (the increase of the catalytic activity for Au and the decrease of the activity for Pt nanoparticles as the diameter decreases). In Fig. 5(b), we plot the two components of the theoretical activity curve for Au, corresponding to the low-coordination and perimeter channels and their sum. The main figure and the inset make clear that the initial rise in the catalytic activity with decreasing Au-nanoparticle size comes from the perimeter channel, as first proposed by Bamwenda *et al.*[2] Below about 3 nm, we start sampling the tail end of the low-coordination-site distribution, which gives a significant boost to the activity. A direct comparison with experimental activities from Ref. 33 for Au nanoparticles supported on TiO_2 (P25), shown in Fig. 5(c), further demonstrates that the theory reproduces the observed size dependence.

Clearly, the above simple model captures the main reaction trends even though it leaves out phenomena such as surface diffusion of reactants and desorption. Some experiments suggest a possible downturn in activity for Au nanoparticles below about 2 nm.[20] Such a downturn may come from "poisoning." For the smallest nanoparticles, most Au atoms have very low coordination, for which the binding energy of both CO and O_2 is high ($E_b \sim 0.7$ eV for O_2 and about 1 eV for CO). Residence times for adsorbates are then very high, and catalytically active sites are blocked.

D. Catalytic activity of bilayer structures

Finally, as many of the particles seen experimentally are around two layers thick, we examined the properties of two

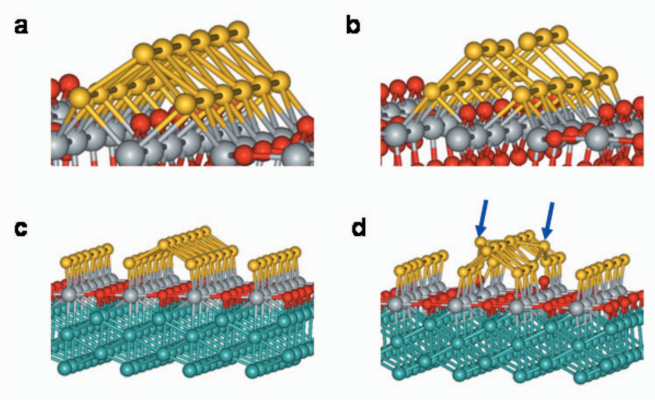

FIG. 6. (Color online) Bilayer Au structures on TiO_2 and on a single TiO_x layer. (a) A Au bilayer structure on the rutile (110) surface with rows of oxygen vacancies. All Au atoms are sixfold and sevenfold coordinated. (b) The top monatomic Au chain in the bilayer structure is unstable against reconstruction, as shown, resulting in itinerant low-coordination sites. (c) Regular bilayer Au structure on a single TiO_x ($x=1$) layer on Mo[112] structure (Mo is shown in turquoise) with compressed Au-Au distances as proposed by Chen and Goodman (Ref. 23). (d) The Au chains buckle when O atoms are introduced under the chains, and low-coordination Au sites (indicated by blue arrows) are created.

different bilayer structures proposed by Goodman and co-workers[23,24] to be responsible for the highest catalytic activity. In the proposed bilayers, the base layer is bonded to a TiO_x layer with unspecified x. We, therefore, investigated several values of x. In Fig. 6(a), we show a schematic of a model of such a structure, comprising Au atoms directly on a TiO_2 substrate. A row of O vacancies is present underneath each first-layer Au chain. The top layer is effectively a collection of slightly stretched Au chains in which the Au atoms have $n=6$. Figure 1(c) suggests low catalytic activity for $n=6$. However, the Au chains are unstable against local reconstruction because the Au-Au spacing imposed by the TiO_2 substrate is ~0.1 Å longer than the Au-Au spacing in bulk Au. Such local reconstruction results in short chains with decreased Au-Au spacing and lower-coordination Au atoms [an example is given in Fig. 6(b)]. The energy gain is small (~0.01 eV per Au atom) so that the low-coordination sites are *itinerant* at room temperature and hence might not be apparent to low-energy electron diffraction. CO and O_2 molecules bind to the low-coordination sites, and the reaction proceeds *with a barrier of only* 0.1 eV. If the underlying rows of O vacancies are incomplete, catalytic activity again occurs because reconstruction results in local environments with low-coordination Au atoms. Similar (1×3) bilayer Pt structures exhibit a very high CO-oxidation reaction barrier for the same reasons as Pt nanoparticles, which would suppress their catalytic activity.

Figure 6(c) shows a schematic of our model for an alternative bilayer structure proposed by Goodman and coworkers, comprising Au atoms on a single TiO_x layer on Mo[112] layers.[23] We found that Au bilayers are compressed for $x\leqslant1$. In this case, the Au-Au distances are 2.73 Å, corresponding to the bulk Mo-Mo distance. These "perfect" Au chains are not catalytically active. When we introduced O atoms in the Ti rows under the Au chains, the chains buckled, creating low-coordination Au sites [Fig. 6(d)] and bond weakening. As was known for Au nanoparticles, O vacancies on the substrate anchor the Au structures, but the net conclusion is that O atoms on the substrate surface cause reconstructions that are responsible for the very high catalytic activity.

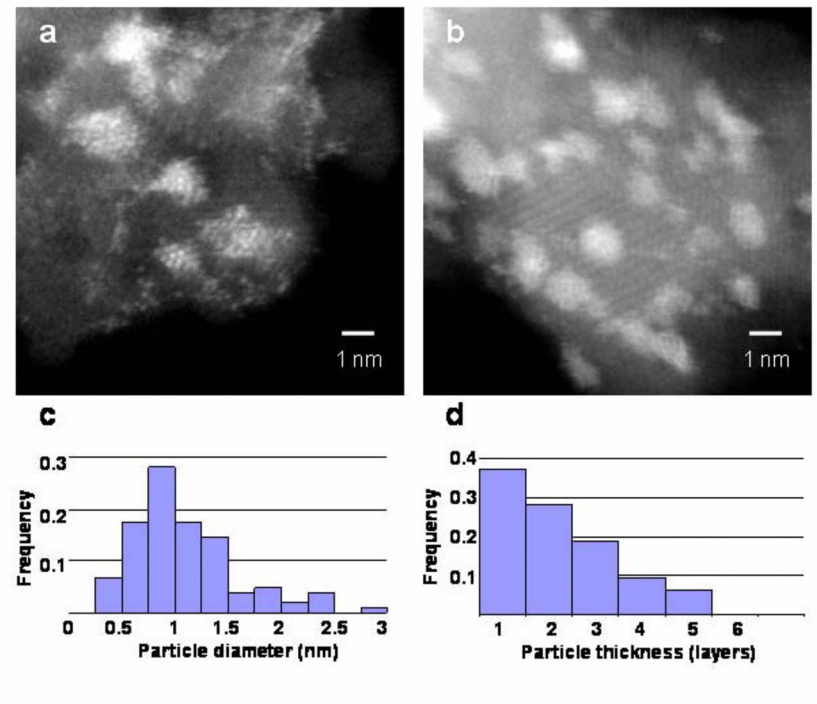

FIG. 7. (Color online) High-magnification *Z*-contrast micrographs showing 10 wt % loaded Au on anatase (from Ref. 39) after two stages of preparation. (a) In the oxidized precursor state following deposition-precipitation of Au, many individual Au atoms are sharply resolved. (b) In the most active form, after mild reduction in 12% H_2 at 423 K, individual neutral Au atoms are not resolved, consistent with structural fluxionality. (c) Histogram of the distribution of 103 Au-particle diameters in the reduced sample. Single atoms and particles over 10 nm were not included. Mean particle size was 1.1 ± 0.5 nm. (d) Histogram of the approximate distribution of 32 selected Au-particle thicknesses in the reduced sample determined from relative intensities of *Z*-contrast images. Most particles are only 1 or 2 layers thick.

E. Atomically resolved *Z*-contrast imaging

We have imaged supported Au nanoparticles using *Z*-contrast scanning transmission electron microscopy and found evidence to corroborate the conclusion that bond weakening or structural fluxionality, necessary for high activity, occurs. In Fig. 7, we show atomic-resolution *Z*-contrast micrographs[38] of samples prepared as part of an experimental investigation of CO oxidation by Au nanoparticles on TiO_2.[39] The micrograph of Fig. 7(a) shows a sample after deposition-precipitation of Au. Individual Au atoms are clearly resolved. In Fig. 7(b), after the sample underwent mild reduction in 12% H_2 at 425 K, individual Au atoms are not well resolved within the nanoparticles, which appear blurred. The difference can be attributed to the oxidized form of the Au (Au hydroxide), which more stably anchors to TiO_2 compared to reduced Au atoms. Thus, our calculations correspond to the reduced nanoparticles of Fig. 7(b). We interpret the fuzziness of Fig. 7(b) as direct imaging of large Au-atom motions, consistent with the weakening of Au–Au bonds found in the present calculations, called dynamic structural fluxionality in earlier work,[18,19] and the low melting point of Au nanoparticles[40] in this size range [Figs. 7(c) and 7(d)]. Most of the nanoparticles in this sample are 1 or 2 layers thick, consistent with the experimental observation[23,24] that the nanoparticle thickness is an important factor in the activity.

IV. CONCLUSIONS

In summary, we have presented a comprehensive theoretical study of the catalytic activity for low-temperature CO oxidation of Au and Pt nanoparticles and bilayer structures on titania, assuming coadsorbed CO and O_2 molecules. We found that for both Au and Pt nanoparticles, the strong adsorption of an O_2 molecule at low-coordination sites causes the O–O bond to be stretched and weakened. We demonstrated that the same nanoscale features act to produce different catalytic behaviors in the two materials primarily because adsorption of the reactants causes bond weakening within Au nanoparticles and bond strengthening within Pt nanoparticles, governing how easily the adsorbed molecules can interact. For Au nanoparticles, we find that perimeter sites are also catalytically active but with a lower reaction barrier, and expect this route to be dominant for larger particles with few low-coordination sites. Finally, we find that the catalytic behavior of Au bilayer structures for CO oxidation appears to be governed by the same phenomena.

ACKNOWLEDGMENTS

Research was sponsored by the Division of Chemical Sciences, Geosciences, and Biosciences, and by the Division of Materials Sciences and Engineering, Office of Basic Energy Sciences, U.S. Department of Energy under Contract No. DE-AC05-00OR22725 with Oak Ridge National Laboratory, managed and operated by UT-Battelle, LLC, and supported in part by the McMinn Endowment at Vanderbilt University. This work was supported in part by a grant of computer time from the DOD High Performance Computing Modernization Program at the Naval Oceanographic Office (NAVO) and the U.S. Army Engineer Research and Development Center (ERDC).

*Present address: Center for Advanced Modeling and Simulation, Idaho National Laboratory, Idaho Falls, ID 83415-2208, USA.
†Corresponding author; FAX: +1 865 574 4143; 9az@ornl.gov

[1] M. Haruta, J. New Mater. Electrochem. Syst. **7**, 163 (2004).
[2] G. R. Bamwenda, S. Tsubota, T. Nakamura, and M. Haruta, Catal. Lett. **44**, 83 (1997).
[3] N. W. Cant, J. Catal. **62**, 173 (1980).
[4] M. Herskowitz, R. Holliday, M. B. Cutlip, and C. N. Kenney, J. Catal. **74**, 408 (1982).
[5] M. Che and C. O. Bennett, Adv. Catal. **36**, 55 (1989).
[6] M. Haruta, S. Tsubota, T. Kobayashi, H. Kageyama, M. J. Genet, and B. Delmon, J. Catal. **144**, 175 (1993).
[7] L. M. Molina and B. Hammer, Phys. Rev. Lett. **90**, 206102 (2003).
[8] I. N. Remediakis, N. Lopez, and J. K. Norskov, Angew. Chem. **44**, 1824 (2005).
[9] I. N. Remediakis, N. Lopez, and J. K. Norskov, Appl. Catal., A **291**, 13 (2005).
[10] N. Lopez, T. V. W. Janssens, B. S. Clausen, Y. Xu, M. Mavrikakis, T. Bligaard, and J. K. Nørskov, J. Catal. **223**, 232 (2004).
[11] N. Lopez, J. K. Nørskov, T. V. W. Janssens, A. Carlsson, A. Puig-Molina, B. S. Clausen, and J.-D. Grunwaldt, J. Catal. **225**, 86 (2004).
[12] N. Lopez and J. K. Norskov, J. Am. Chem. Soc. **124**, 11262 (2002).
[13] Z. P. Liu, X. Q. Gong, J. Kohanoff, C. Sanchez, and P. Hu, Phys. Rev. Lett. **91**, 266102 (2003).
[14] Z. P. Liu and P. Hu, Top. Catal. **28**, 71 (2004).
[15] Z. P. Liu, P. Hu, and A. Alavi, J. Am. Chem. Soc. **124**, 14770 (2002).
[16] L. M. Molina, M. D. Rasmussen, and B. Hammer, J. Chem. Phys. **120**, 7673 (2004).
[17] L. M. Molina and B. Hammer, Appl. Catal., A **291**, 21 (2005).
[18] B. Yoon, H. Hakkinen, and U. Landman, J. Phys. Chem. A **107**, 4066 (2003).
[19] B. Yoon, H. Hakkinen, U. Landman, A. S. Worz, J.-M. Antonietti, S. Abbet, K. Judai, and U. Heiz, Science **307**, 403 (2005).
[20] M. Valden, X. Lai, and D. W. Goodman, Science **281**, 1647 (1998).
[21] M. Valden, S. Pak, X. Lai, and D. W. Goodman, Catal. Lett. **56**, 7 (1998).
[22] J. Guzman and B. C. Gates, J. Am. Chem. Soc. **126**, 2672 (2004).
[23] M. S. Chen and D. W. Goodman, Science **306**, 252 (2004).
[24] M. Chen, Y. Cai, Z. Yan, and D. W. Goodman, J. Am. Ceram. Soc. **128**, 6341 (2006).
[25] E. Wahlstrom, N. Lopez, R. Schaub, P. Thostrup, A. Rønnau, C. Africh, E. Lægsgaard, J. K. Nørskov, and F. Besenbacher, Phys.

Rev. Lett. **90**, 026101 (2003).
[26] M. C. Payne, M. P. Teter, D. C. Allan, T. A. Arias, and J. D. Joannopoulos, Rev. Mod. Phys. **64**, 1045 (1992).
[27] J. P. Perdew, K. Burke, and M. Ernzerhof, Phys. Rev. Lett. **77**, 3865 (1996).
[28] G. Kresse and J. Hafner, Phys. Rev. B **48**, 13115 (1993); G. Kresse and J. Furthmüller, *ibid.* **54**, 11169 (1996).
[29] D. J. Chadi and M. L. Cohen, Phys. Rev. B **8**, 5747 (1973).
[30] H. Johnson, G. Mills, and K. W. Jacobsen, in *Classical and Quantum Dynamics in Condensed Phase Systems*, edited by B. J. Berne, G. Cicotti, and D. F. Coker (World Scientific, River Edge, NJ, 1998).
[31] A. Eichler and J. Hafner, Phys. Rev. B **59**, 5960 (1999).
[32] A. Alavi, P. J. Hu, T. Deutsch, P. L. Silvestrelli, and J. Hutter, Phys. Rev. Lett. **80**, 3650 (1998).
[33] S. H. Overbury, V. Schwartz, D. R. Mullins, W. F. Yan, and S. Dai, J. Catal. **241**, 56 (2006).
[34] T. V. W. Janssens, A. Carlsson, A. Puig-Molina, and B. S. Clausen, J. Catal. **240**, 108 (2006).
[35] R. S. Mulliken, J. Chem. Phys. **23**, 1833 (1955).
[36] R. F. W. Bader, Acc. Chem. Res. **8**, 34 (1975); **18**, 9 (1985); *Atoms in Molecules: A Quantum Theory* (Oxford University Press, Oxford, 1990).
[37] C. H. Perrin, J. Am. Chem. Soc. **113**, 2865 (1991).
[38] S. J. Pennycook and D. E. Jesson, Phys. Rev. Lett. **64**, 938 (1990).
[39] W. F. Yan, B. Chen, S. M. Mahurin, V. Schwarz, D. R. Mullins, A. R. Lupini, S. J. Pennycook, S. Dai, and S. H. Overbury, J. Phys. Chem. B **109**, 10676 (2005).
[40] P. Buffat and J. P. Borel, Phys. Rev. A **13**, 2287 (1976).